REPORT

SUPERCONDUCTIVITY

Evidence for bulk superconductivity in pure bismuth single crystals at ambient pressure

Om Prakash, Anil Kumar, A. Thamizhavel, S. Ramakrishnan*

At ambient pressure, bulk rhombohedral bismuth is a semimetal that remains in the normal state down to at least 10 millikelvin. Superconductivity in bulk bismuth is thought to be unlikely because of the extremely low carrier density. We observed bulk superconductivity in pure bismuth single crystals below 0.53 millikelvin at ambient pressure, with an estimated critical magnetic field of 5.2 microteslas at 0 kelvin. Superconductivity in bismuth cannot be explained by the conventional Bardeen-Cooper-Schrieffer theory because its adiabatic approximation does not hold true for bismuth. Future theoretical work will be needed to understand superconductivity in the nonadiabatic limit in systems with low carrier densities and unusual band structures, such as bismuth.

Bismuth (Bi) has played an important role in uncovering many interesting phenomena in condensed matter research (1–3), such as the Seebeck, Nernst (4), Shubnikov–de Haas, and de Haas–van Alphen (dHvA) effects (5). Its anomalous electronic properties continue to draw considerable scientific interest (6–13). The determination of the Fermi surface in Bi from dHvA measurements (14) provided the basis to determine the Fermi surfaces of other compounds. The rhombohedral crystal structure of Bi, which can be derived by distorting a cubic structure, leads to a number of quantum phenomena (15, 16). Some of the key properties of Bi are a small density of states (DOS; 4.2×10^{-6} states eV^{-1} $atom^{-1}$) at the Fermi level, a very small Fermi surface (~10^{-5} of the Brillouin zone, consisting of small electron and hole pockets), low Fermi energy ($E_F \approx 25$ meV), low carrier density ($n \approx 3 \times 10^{17}$ cm^{-3} at 4.2 K), and small effective mass for charge carriers ($m_{eff} \approx 10^{-3}$ m_e, where m_e is the free electron mass) (17, 18). The low Fermi energy in Bi results in a large electronic mean free path exceeding 2 μm at 300 K, because slow electrons are prevented by the conservation laws from interacting with any but the longest lattice vibrations (19–21). Generally, at low temperatures, the electronic mean free path is limited by scattering due to defects. In Bi, because of the long Fermi wavelength (10 to 50 nm), the carriers are not scattered by point defects or atomic impurities. The long mean free path in Bi is instead limited by extended defects such as dislocations. In addition, thanks to the small n, the Coulomb screening (μ*) in Bi

is much weaker than that in metals such as Au, Cu, Al, and others.

The search for superconductivity in bulk Bi began more than half a century ago. Although superconductivity was observed at high pressures in amorphous forms, thin films, metal heterostructures, granular nanowires, and nanoparticles of Bi, bulk Bi under ambient conditions remained in the normal state down to 10 mK (7, 12, 22–24). Here we report bulk superconductivity in pure Bi single crystals (99.998%) below 0.53 mK, observed by measuring the Meissner effect (diamagnetic) by means of a gradiometer coil coupled with a dc SQUID (superconducting quantum interference device). The Bi single crystals were grown using the Bridgman crystal growth technique and characterized using energy dispersive x-ray spectroscopy, powder x-ray diffraction, and Laue diffraction (figs. S1 to S3) (25). In addition, the inductively coupled plasma–atomic emission spectrometry (ICP-AES) technique was used to estimate the trace impurities in Bi crystals (25). The ICP-AES results show that our crystals have extremely low impurity levels (table S1). This is further confirmed by the quantum oscillation measurements (fig. S6 and table S2).

For the measurements, Bi crystals ($2 \times 0.2 \times 0.2$ cm^3) were attached to an annealed high-purity silver (Ag) rod (99.999%), which was threaded to the copper (Cu) nuclear stage (Fig. 1A). Rectangular holes ($0.6 \times 0.3 \times 0.3$ cm^3) were made in the Ag rods, and Bi crystals were push-fitted in the holes, along with fine Ag powder for tight sealing. Subsequently, the Ag rod was crimped to hold the samples tight, ensuring a good thermal contact. The measurement setup consisted of a compensated first-order symmetric gradiometer pickup coil and an excitation coil, both made of superconducting niobium (Nb) wires. The gradiometer assembly comprised an astatic pair of coils (four turns each) with a distance of

1.2 cm between them. The cross section of the gradiometer coils was minimized to fit the sample and maximize the filling fraction. The gradiometer coils were connected to the input coil of the dc SQUID (25). The primary coils were wound on a former made from stycast. The whole measurement setup (excitation and pickup coils) was enclosed in magnetic shielding consisting of a high-permeability material called Cryoperm 10 and superconducting lead (Pb) shields. This magnetic shielding arrangement is capable of reducing the external magnetic fields to less than 10 nT at 4.2 K (Fig. 1B), when there is no current in the primary coil. Apart from reducing the effect of external magnetic fields, the magnetic shielding also affects the field inside, owing to the primary coil. For this reason, we calibrated the primary coils enclosed in the magnetic shielding at 4.2 K by using a very sensitive single-axis magnetometer with a low field probe (±1-nT resolution) so as to precisely control the excitation magnetic fields during the measurements. The shielded excitation coil setup was mounted at the bottom of the mixing chamber plate of the dilution refrigerator (Fig. 1B). The pickup coil was connected to the dc SQUID (Fig. 1C), which in turn was connected to the radio frequency (RF) amplifier fixed at the head of the cryostat at room temperature. The RF head was connected to the SQUID control unit, which directly reads output in volts. The dc SQUID output was calibrated at 4.2 K by measuring the diamagnetic signal from the conventional superconductors Nb and Pb. One of the main challenges in using this method is to calibrate the SQUID output voltage with respect to the susceptibility (Meissner signal). To resolve this, we used Pb samples of the same dimensions as the Bi samples and measured the jump in the SQUID output voltage at the transition temperature T_C with different excitation fields (see fig. S7). For the calibration, we used the same experimental setup described above and the same excitation fields as used during the measurement of Bi.

The following two requirements have to be fulfilled to observe superconductivity in superconductors with extremely low T_C. (i) The sample environment has to be very well shielded from the external magnetic fields, because superconductors with extremely low T_C inevitably have very small critical fields. Any background magnetic field in the vicinity of the sample can easily suppress the superconducting T_C to even lower temperatures. (ii) The sample has to be free from magnetic impurities, because the presence of magnetic impurities can also suppress the superconductivity. Apart from these two requirements, the Bi samples need to be extremely pure with no doping. Doping in Bi increases the DOS at the Fermi level and can induce superconductivity (26). The values of the Hall coefficient R_H for our single crystals, measured using the Physical Properties Measurement System (Quantum Design), were 0.5 cm^3 C^{-1} (at magnetic field $H = 0.1$ T) at 300 K and 3.5 cm^3 C^{-1} ($H = 0.1$ T) at 4.2 K (fig. S4A) (25), which are in

Department of Condensed Matter Physics and Material Sciences, Tata Institute of Fundamental Research, Mumbai 400005, India.
*Corresponding author. Email: ramky@tifr.res.in

agreement with the values reported in literature [27], suggesting the absence of doping in our crystals. The estimated Sommerfeld constant for Bi from heat capacity measurements (fig. S4B), $\gamma \approx 5$ μJ mol^{-1} K^{-2} at 100 mK, agrees well with previously reported values [28] and reflects the high purity of the Bi crystals. The resistivity of the Bi crystals at 300 K [25], $\rho = 129 \pm 0.2$ microohm·cm, is also in agreement with the previously reported values for undoped Bi. The resistivity of all the crystals at 4.2 K is less than 0.3 ± 0.02 microohm·cm (fig. S5). The resistivity was measured on much thicker crystal (thickness, 6.1 mm) than that used in the magnetization measurements to avoid size effects on resistivity [29]. The resistivity of thinner Bi crystal is limited by boundary scattering due to a large electronic mean free path [29]. The residual resistivity ratio of grown samples at 4.2 K is ≥430, indicating the high quality of the single crystals (fig. S5). The carrier density $n \approx 3 \times 10^{17}$ cm^{-3} and the resistivity $\rho < 0.3 \pm 0.02$ microohm·cm at 4.2 K imply a mobility $\mu_e \geq 3.5 \times 10^7$ cm^2 V^{-1} s^{-1}, by far the largest known in any solid.

The experiment was performed in a dilution refrigerator equipped with a Cu adiabatic demagnetizing stage. The Cu stage was first cooled by the dilution refrigerator to 5 mK; this was followed by magnetization of the Cu nuclear spins by using a superconducting magnet to apply a magnetic field of 9 T. The Cu stage was thermally connected to the mixing chamber by using an aluminum (Al) superconducting thermal switch to facilitate isothermal magnetization. The application of the 9-T magnetic field heated the Cu stage to nearly 40 mK owing to the heat of magnetization, and we had to wait for nearly 36 hours for the magnetized Cu stage to cool to

10 mK. Subsequently, to thermally disconnect the Cu stage from the mixing chamber, the Al thermal switch was turned off by turning off the current in the solenoid enclosing it. A slow adiabatic demagnetization of Cu nuclear spins over a period of 48 hours cooled the Cu stage to a base temperature of 100 μK. Slow demagnetization helped in maintaining thermal equilibrium between the samples and the Cu stage, as well as with the nuclear magnetic resonance (NMR) thermometer. We used a platinum-195 (^{195}Pt) NMR thermometer for the temperature measurements below 10 mK during adiabatic demagnetization. The NMR thermometer was calibrated against the cerium magnesium nitrate (paramagnetic) thermometer and the SQUID-based noise thermometer at 10 mK. The SQUID-based noise thermometer can also measure temperatures down to 1 mK and was used along with the NMR thermometer below 10 mK. The details of the adiabatic nuclear refrigerator, temperature measurement, and calibration are given in [30].

The superconducting transitions for two Bi samples, s1 and s2 (from two different growth batches), were observed below 0.53 mK in an excitation field of 0.4 μT in the form of a sharp drop in the dc susceptibility as a function of temperature [$\chi_v(T)$] (Fig. 2A). The $\chi_v(T)$ data for s1 in the zero field–cooled (ZFC) and field-cooled (FC) states suggest the absence of a vortex state (i.e., vortex pinning), indicating type I superconductivity in Bi. The FC data for s2 is in good agreement with that for s1 at the same excitation field of 0.4 μT (Fig. 2A). The $\chi_v(T)$ for both s1 and s2 was measured in different magnetic fields (Fig. 2B). The superconductivity transition shifts toward lower temperatures with

increasing field. The transition temperatures at different magnetic fields are shown in Fig. 2C. The data in Fig. 2C are fitted to $H_C(T) = H_C(0)[1-(T/T_C)^2]$ to estimate the value of the critical field H_C at 0 K. The critical field estimated from the fit is 5.2 ± 0.1 μT. All measurements were performed on the free end of the samples, nearly 1 cm away from the Ag rod [25], avoiding artifacts caused by the interface effects.

We calibrated the measurement setup with superconducting Pb and rhodium (Rh) samples of about the same dimensions. The magnitude of the Meissner signal (the jump in the SQUID voltage) observed for Bi is nearly the same as the diamagnetic signal observed for superconducting Pb and Rh in the same excitation field of 0.4 μT, suggesting that a large volume fraction (bulk) of Bi crystal underwent the superconducting transition. The extrapolated critical field at 0 K for Bi [$H_C(0) = 5.2 \pm 0.1$ μT] is similar to the critical field for Rh [31], even though the Fermi velocity v_F, DOS at the Fermi level, and carrier density in Bi are all very small compared with those in Rh. The Fermi velocity of Bi was calculated as $v_F = (\hbar/m_e)(3\pi^2 n)^{1/3}$, where n is the carrier density and $\hbar$ is the Dirac constant (also known as the reduced Planck constant). Taking $n \approx 3 \times 10^{17}$ cm^{-3}, we obtained $v_F = 2.4 \times 10^6$ cm s^{-1} for Bi, which is two orders of magnitude smaller than the Fermi velocity in Rh.
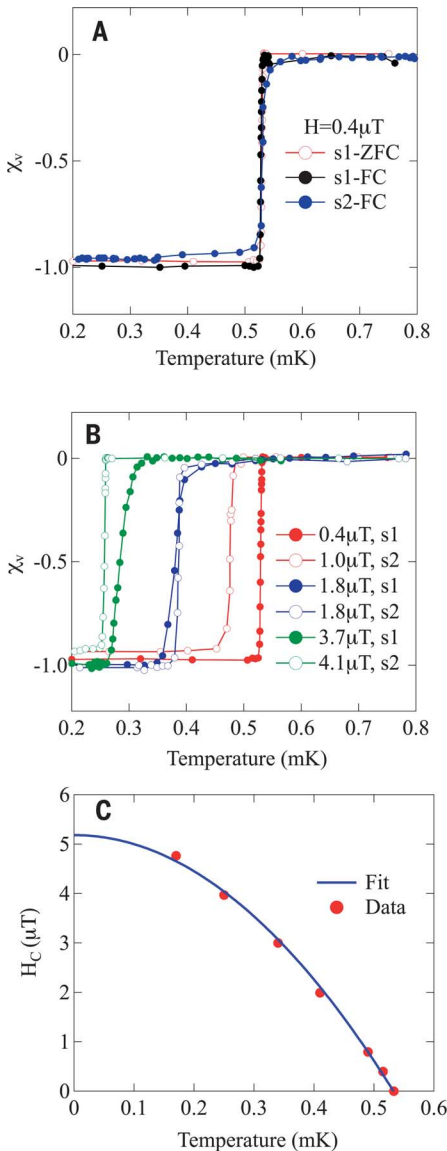
To understand whether the superconductivity in Bi is dirty or clean, we estimated the superconducting coherence length with the formula $\xi_0 = \hbar v_F/3.52 k_B T_C$, assuming the Bardeen-Cooper-Schrieffer (BCS) framework (where k_B is the Boltzmann's constant). We found $\xi_0 = 96$ μm when using the values of v_F and T_C for Bi. Because
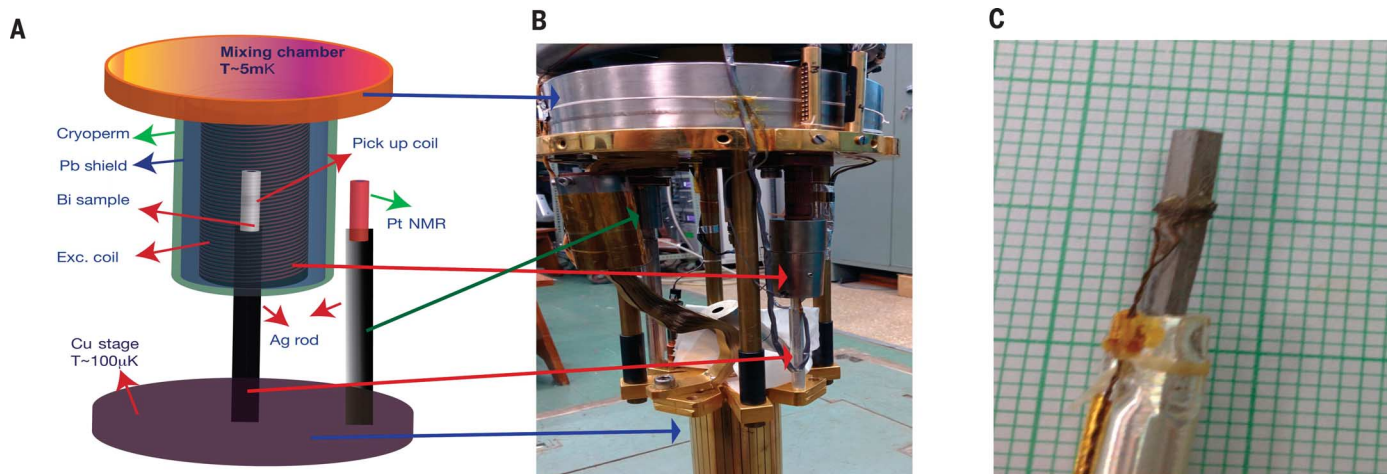
Fig. 1. Schematic diagram of the magnetic shields and measurement setup. (**A**) The measurement setup consists of an excitation coil (0.04 μT/μA) enclosed in a magnetically shielded environment. The magnetic shielding consists of four layers of Pb foil inside two layers of Cryoperm 10 cylindrical shields. This setup can shield the sample from the external magnetic fields down to 10 nT. The excitation coil and the shielding are attached to the mixing chamber plate of the dilution refrigerator ($T \approx 5$ mK). The sample is push-fitted and pinched in an Ag rod attached to the low-temperature Cu stage ($T \approx 100$ μK).

A similar mounting arrangement was used for the ^{195}Pt NMR thermometer, as shown in the diagram. A gradiometer pickup coil was directly wound on the crystal and connected to the input coil of the dc SQUID. We used two identical setups with different Bi crystals for the measurements. (**B**) Photograph of the actual measurement setup in the dilution insert. The arrows mark different components shown in the diagram. (**C**) A Bi single crystal attached to the Ag rod. The pickup coil is wound directly on the crystal and connected to the input terminals of the dc SQUID.

the mean free path of Bi as estimated from the resistivity measurements is ~300 μm at 4.2 K, Bi can be classified as a clean type I superconductor. The BCS model also gives the relation $B_C(0)/T_C = (\mu_0\gamma/2V_M)^{1/2}$, where B_C is critical field, μ_0 is the vacuum permeability, γ is the electronic specific heat coefficient in the normal state, and V_M is the molar volume. Using the normal state parameters of Bi, we estimated this ratio to be equal to 0.79 mT K^{-1}, in contrast to the experimental value of 9.4 mT K^{-1}, indicating the inapplicability of the standard BCS theory (32). We roughly estimated ξ_0 by using the BCS formula so that we could compare it with the mean free path; the actual value of ξ_0 might be different from the value estimated above.

Superconductivity in metallic elements can be understood from the BCS theory (32) and its extensions, and the transition temperature is given by $T_C = \Theta_D\exp[-1/N(0)V]$, where Θ_D, $N(0)$, and V are the Debye temperature, electronic DOS at E_F, and phonon-mediated attractive electron-electron interaction, respectively. However, even though electron-phonon interaction occurs in Bi, the conventional BCS model cannot be applied to Bi. Bi has a multivalley band structure and small DOS at the Fermi level. Studying the importance of the multivalley band structure in systems with low carrier densities, such as Bi, Cohen showed that the attractive electron-electron interaction arising from the exchange of intravalley and intervalley phonons can be larger than the repulsive Coulomb interaction in many-valley semiconductors and semimetals, and it can cause these materials to exhibit superconducting properties (33).

The Fermi energy $E_F \approx 25$ meV is comparable to the phonon energy $\hbar\omega_D \approx 12$ meV in Bi, where ω_D is the Debye frequency (34). The BCS theory of superconductivity is formulated in the so-called adiabatic limit, $\omega_D/E_F \ll 1$. This assumption is clearly violated for Bi, given that $\omega_D/E_F \approx 0.5$. Many known superconductors, such as SrTiO$_{3-\delta}$, fullerene (C$_{60}$) compounds, and superconducting semiconductors, have $E_F \leq \hbar\omega_D$. Several attempts have been made to extend the BCS theory to account for superconductivity in these systems in the nonadiabatic limit (35–40). Some other theories on the mechanism of superconductivity, based on purely electronic correlations, also exist (41, 42) but cannot be applied to systems with low carrier densities like Bi. The estimated T_C for Bi based on the BCS theory and its extensions is orders of magnitude smaller (in the picokelvin range) than the observed T_C of 0.53 mK.

In the nonadiabatic limit, $\omega_D/E_F \geq 1$, Migdal's theorem breaks down and requires the inclusion of vertex renormalization and higher-order diagrams in the self-consistent gap equation (37). The nonadiabatic effects produce strong enhancement in T_C with respect to the usual Migdal-Eliashberg theory (43, 44). In particular, (38) generalized the many-body theory of superconductivity in a perturbative scheme with respect to the parameter $\lambda\omega_D/E_F$, where λ is the electron-phonon coupling constant, by calculating the vertex correction function and self energy in the nonadiabatic limit. They found that the vertex correction function behaves in a complex way with respect to the momentum **q** and frequency ω of the exchange phonon. Specifi-

cally, the vertex corrections are positive for small values of **q** and can lead to strong enhancement of T_C, as compared with the usual BCS theory. In this case, the superconducting transition temperature is given by $T_C = 1.13\Theta_D e^{-1/\lambda(1+\lambda)-\mu^*}$ (in the usual BCS theory, $T_C = 1.13\Theta_D e^{-1/\lambda-\mu^*}$). Using the Coulomb screening $\mu^* = 0.105$ (45) and the observed $T_C = 0.53$ mK in $T_C = 1.13\Theta_D e^{-1/\lambda(1+\lambda)-\mu^*}$, we obtained $\lambda = 0.16$, suggesting rather weak electron-phonon coupling in Bi. This value of λ is similar to but smaller than the value estimated for crystalline Bi in a recent simulation study (46).

In systems with low carrier densities and multivalley electronic structures (as is the case for Bi), Cohen (46) showed that intervalley electron-phonon interactions contribute considerably to the net attractive electronic potential. The intervalley scattering is associated with large momentum transfer, whereas the calculations (38) show that the enhancement in T_C caused by vertex corrections happens at small **q**. Although the superconductivity in Bi can be qualitatively explained by the model in (38), new theoretical inputs are needed to estimate the superconducting parameters in systems with low carrier densities in the nonadiabatic limit.

REFERENCES AND NOTES

1. A. H. Wilson, *Proc. R. Soc. Lond. A* **138**, 594–606 (1932).
2. N. F. Mott, H. Jones, *The Theory of the Properties of Metals and Alloys* (Dover Publications, 1958).
3. V. Édel'man, *Adv. Phys.* **25**, 555–613 (1976).
4. A. v. Ettingshausen, W. Nernst, *Ann. Phys. Chem.* **265**, 343–347 (1886).
5. Y. Fuseya, M. Ogata, H. Fukuyama, *J. Phys. Soc. Jpn.* **84**, 012001 (2015).
6. L. Li *et al.*, *Science* **321**, 547–550 (2008).
7. M. Tian *et al.*, *Nano Lett.* **6**, 2773–2780 (2006).
8. F. Y. Yang *et al.*, *Science* **284**, 1335–1337 (1999).
9. K. Behnia, M.-A. Méasson, Y. Kopelevich, *Phys. Rev. Lett.* **98**, 166602 (2007).
10. J. Heremans *et al.*, *Phys. Rev. B* **61**, 2921–2930 (2000).
11. J. Heremans *et al.*, *Phys. Rev. B* **58**, R10091–R10095 (1998).
12. B. Weitzel, H. Micklitz, *Phys. Rev. Lett.* **66**, 385–388 (1991).
13. F. M. Muntyanu, A. Gilewski, K. Nenkov, J. Warchulska, A. J. Zaleski, *Phys. Rev. B* **73**, 132507 (2006).
14. D. Shoenberg, *Proc. R. Soc. Lond. A* **170**, 341 (1939).
15. J. W. Wells *et al.*, *Phys. Rev. Lett.* **102**, 096802 (2009).
16. K. Behnia, L. Balicas, Y. Kopelevich, *Science* **317**, 1729–1731 (2007).
17. Y. Liu, R. E. Allen, *Phys. Rev. B* **52**, 1566–1577 (1995).
18. G. E. Smith, G. A. Baraff, J. M. Rowell, *Phys. Rev.* **135**, A1118–A1124 (1964).
19. E. H. Sondheimer, *Proc. Phys. Soc. A* **65**, 562–564 (1952).
20. A. B. Pippard, R. G. Chambers, *Proc. Phys. Soc. A* **65**, 955–956 (1952).
21. R. Hartman, *Phys. Rev.* **181**, 1070–1086 (1969).
22. T. Hamada, K. Yamakawa, F. E. Fujita, *J. Phys. F Met. Phys.* **11**, 657–670 (1981).
23. M. Tian *et al.*, *Nano Lett.* **9**, 3196–3202 (2009).
24. P. J. Hakonen, G. Nunes Jr., *J. Phys. Condens. Matter* **3**, 7153–7160 (1991).
25. Materials and methods are available as supplementary materials.
26. C. Uher, J. L. Opsal, *Phys. Rev. Lett.* **40**, 1518–1521 (1978).
27. J. P. Michenaud, J. P. Issi, *J. Phys. C Solid State Phys.* **5**, 3061–3072 (1972).
28. N. E. Phillips, *Phys. Rev.* **118**, 644–647 (1960).
29. I. N. Zhilyaev, L. P. Mezhov-Deglin, *Sov. Phys. JETP* **43**, 507 (1976).

Fig. 2. Observation of superconductivity, the Meissner effect, and the critical field $H_C(T)$ in Bi single crystals. (**A**) The dc susceptibility as a function of temperature [$\chi_v(T)$] for samples s1 and s2. A sharp drop in the susceptibility at 0.53 mK marks the transition into the superconducting state. FC, field-cooled; ZFC, zero field–cooled. (**B**) $\chi_v(T)$ at different magnetic fields. The data corresponding to the 1.8-μT magnetic field show the transition at 0.37 mK for both samples s1 and s2. (**C**) Phase diagram of the critical magnetic field $H_C(T)$ versus critical temperature (T_C) for Bi. The data are fitted to $H_C(T) = H_C(0)[1 - (T/T_C)^2]$, and the extrapolated critical magnetic field value is $H_C(0) = 5.2 \pm 0.1$ μT.

30. H. R. Naren, R. S. Sannabhadti, A. Kumar, V. Arolkar, S. Ramakrishnan, . *AIP Conf. Proc.* **1447**, 503 (2012).
31. C. Buchal, F. Pobell, R. M. Mueller, M. Kubota, J. R. Owers-Bradley, *Phys. Rev. Lett.* **50**, 64–67 (1983).
32. J. Bardeen, L. N. Cooper, J. R. Schrieffer, *Phys. Rev.* **108**, 1175–1204 (1957).
33. M. L. Cohen, *Phys. Rev.* **134**, A511–A521 (1964).
34. H. J. Zeiger *et al.*, *Phys. Rev. B* **45**, 768–778 (1992).
35. L. P. Gor'kov, *Phys. Rev. B* **93**, 054517 (2016).
36. X. Lin *et al.*, *Phys. Rev. Lett.* **112**, 207002 (2014).
37. L. Pietronero, S. Strässler, *Europhys. Lett.* **18**, 627 (1992).
38. L. Pietronero, S. Strässler, C. Grimaldi, *Phys. Rev. B* **52**, 10516–10529 (1995).
39. C. S. Koonce, M. L. Cohen, J. F. Schooley, W. R. Hosler, E. R. Pfeiffer, *Phys. Rev.* **163**, 380–390 (1967).
40. C. S. Koonce, M. L. Cohen, *Phys. Rev.* **177**, 707–719 (1969).
41. W. Kohn, J. M. Luttinger, *Phys. Rev. Lett.* **15**, 524–526 (1965).
42. J. M. Luttinger, *Phys. Rev.* **150**, 202–214 (1966).
43. A. Migdal, *Sov. Phys. JETP* **34**, 1438 (1958).
44. G. Éliashberg, *Sov. Phys. JETP* **11**, 696 (1960).
45. Z. Mata-Pinzón, A. A. Valladares, R. M. Valladares, A. Valladares, *PLOS ONE* **11**, e0147645 (2016).
46. M. Cohen, in *Superconductivity*, vols. 1 and 2, R. D. Parks, Ed. (Marcel Dekker, 1969), pp. 615–664.

Science

Evidence for bulk superconductivity in pure bismuth single crystals at ambient pressure
Om Prakash, Anil Kumar, A. Thamizhavel and S. Ramakrishnan

Going cold with Bismuth
Many elemental metals, such as lead and aluminum, become superconducting at low temperatures. Bismuth, a semimetal with very low carrier density, stays nonsuperconducting down to 10 mK. Prakash *et al.* performed tricky magnetization measurements to show that pure bulk bismuth does undergo the superconducting transition at a tiny temperature of about 0.5 mK (see the Perspective by Behnia). Because bismuth does not fit neatly into the standard picture of superconductivity, further theoretical work is necessary to explain the findings.
Science, this issue p. 52; see also p. 26

ARTICLE TOOLS	http://science.sciencemag.org/content/355/6320/52
SUPPLEMENTARY MATERIALS	http://science.sciencemag.org/content/suppl/2016/11/30/science.aaf8227.DC1
RELATED CONTENT	http://science.sciencemag.org/content/sci/355/6320/26.full
REFERENCES	This article cites 48 articles, 5 of which you can access for free http://science.sciencemag.org/content/355/6320/52#BIBL
PERMISSIONS	http://www.sciencemag.org/help/reprints-and-permissions

Use of this article is subject to the Terms of Service